Fluorescence relaxation in the near-field of a mesoscopic metallic particle : distance dependence and role of plasmon modes

Gérard Colas Des Francs, Alexandre Bouhelier, Eric Finot, Jean-Claude Weeber, Alain Dereux, Christian Girard, Erik Dujardin

Fluorescence relaxation in the near–field of a mesoscopic metallic particle: distance dependence and role of plasmon modes

G. Colas des Francs[1], A. Bouhelier[1], E. Finot[1], J. C. Weeber[1], A. Dereux[1], C. Girard[2] and E. Dujardin[2]

[1]*Institut Carnot de Bourgogne, UMR 5209 CNRS - Université de Bourgogne, 9 Av. A. Savary, BP 47 870, 21078 Dijon, FRANCE*

[2]*Centre d'Elaboration de Matériaux et d'Etudes Structurales (CNRS) 29, rue Jeanne Marvig BP 4347, F-31055 Toulouse, FRANCE*

**Corresponding author: gerard.colas-des-francs@u-bourgogne.fr*

Abstract: We analytically and numerically analyze the fluorescence decay rate of a quantum emitter placed in the vicinity of a spherical metallic particle of mesoscopic size (*i.e* with dimensions comparable to the emission wavelength). We discuss the efficiency of the radiative decay rate and non–radiative coupling to the particle as well as their distance dependence. The electromagnetic coupling mechanisms between the emitter and the particle are investigated by analyzing the role of the plasmon modes and their nature (dipole, multipole or interface mode). We demonstrate that near-field coupling can be expressed in a simple form verifying the optical theorem for each particle modes.

OCIS codes: (260.2510) Fluorescence;(260.2160) Energy transfer;(240.6680) Surface plasmons

References and links

1. R. P.Van Duyne, Molecular plasmonics, Science **306**, 985 (2004).
2. D. W. Pohl, "Near-field optics seen as an antenna problem," in *Near-field Optics, Principles and Applications*, X. Zhu and M. Ohtsu, eds., pp. 9–21. (World Scientific, Singapore, 2000).
3. P. Mühlschlegel, H.-J. Eisler, O. J. F. Martin, B. Hecht, and D. W. Pohl, "Resonant Optical Antennas," Science **308**, 1607 – 1609 (2005).
4. T. H. Taminiau, R. J. Moerland, F. B. Segerink, L. Kuipers, and N. F. van Hulst, "$\lambda/4$ resonance of an optical monopole antenna probed by single molecule fluorescence," Nano Lett. **7**, 28–33 (2007).
5. D. Chang, A. Sörensen, P. Hemmer, and M. Lukin, "Quantum Optics with Surface Plasmons," Phys. Rev. Lett. **97**, 053002 (2006).
6. L. A. Blanco and F. J. G. de Abajo, "Spontaneous light emission in complex nanostructures," Phys. Rev. B **69**, 205414 (2004).
7. P. Anger, P. Bharadwaj, and L. Novotny, "Enhancement and quenching of single molecule fluorescence," Phys. Rev. Lett. **96**, 113002 (2006).
8. T. Härtling, P. Reichenbach, and L. M. Eng, "Near-field coupling of a single fluorescent molecule and a spherical gold nanoparticle," Opt. Express **15**, 12806–12817 (2007).
9. L. Rogobete, F. Kaminski, M. Agio, and V. Sandoghdar, "Design of nanoantennae for the enhancement of spontaneous emission," Opt. Lett. **32**, 1623–1625 (2007).
10. G. Baffou, C. Girard, E. Dujardin, G. Colas des Francs, and O. Martin, "Molecular quenching and relaxation in a plasmonic tunable nanogap," Phys. Rev. B **77**, 121101(R) (2008).

#98208 - $15.00 USDReceived 1 Jul 2008; revised 22 Aug 2008; accepted 24 Aug 2008; published 17 Oct 2008

11. E. Dulkeith, A. C. Morteani, T. Niedereichholz, T. A. Klar, J. Feldmann, S. A. Levi, F. C. J. M. van Veggel, D. N. Reinhoudt and M. Möller, and D. I. Gittins, "Fluorescence Quenching of Dye Molecules near Gold Nanoparticles: Radiative and Nonradiative Effects," Phys. Rev. Lett. **89**, 203002 (2002).
12. S. Kühn, U. Hakanson, L. Rogobete, and V. Sandoghdar, "Enhancement of single molecule fluorescence using a gold nanoparticle as an optical nano-antenna," Phys. Rev. Lett. **97**, 017402 (2006).
13. P. Bharadwaj and L. Novotny, "Spectral dependence of single molecule fluorescence enhancement," Opt. Express **15**, 14266–14274 (2007).
14. H. Mertens, A. Koenderink, and A. Polman, "Plasmon-enhanced luminescence near noble-metal nanospheres: Comparison of exact theory and an improved Gersten and Nitzan model," Phys. Rev. B **76**, 115123 (2007).
15. V. Klimov, M. Ducloy, and V. S. Letokhov, "Radiative Frequency Shift and Line Width of an Atom Dipole in the Vicinity of a Dielectric Microsphere," J. Mod. Opt. **43**, 2251 (1996).
16. P. T. Leung, "Decay of molecules at spherical surfaces: Nonlocal effects," Phys. Rev. B **42**, 7622 (1990).
17. C. Girard, S. Maghezzi, and F. Hache, "Multipolar propagators near a small metallic sphere : A self consistent calculation," J. Chem. Phys. **91**, 5509–5517 (1989).
18. C. Bohren and D. Huffman, *Absorption and scattering of light by small particles* (1983).
19. Y. S. Kim, P. T. Leung, and T. F. George, "Classical Decay Rates for Molecules in the Presence of a Spherical Surface: a Complete Treatment," Surf. Sci. **195**, 1–14 (1988).
20. H. Chew, "Transitions rates of atoms near spherical surfaces," J. Chem. Phys. **87**, 1355–1360 (1987).
21. M. Abramowitz and I. Stegun, *Hanbbook of mathematical functions* (Dover Publications, 1972).
22. G. Colas des Francs, C. Girard, M. Juan, and A. Dereux, "Energy transfer in near-field optics," J. Chem. Phys. **123**, 174709 (2005).
23. R. Carminati, J. Greffet, C. Henkel, and J. Vigoureux, "Radiative and non-radiative decay of a single molecule close to a metallic nanoparticle," Opt. Commun. **261**, 368–375 (2006).
24. R. R. Chance, A. Prock, and R. Silbey, "Molecular fluorescence and energy transfer near interfaces," Adv. Chem. Phys. **37**, 1–65 (1978).
25. M. Meier and A. Wokaun, "Enhanced fields on large metal particles: dynamic depolarization," Opt. Lett. **8**, 581 (1983).
26. G. Colas des Francs, C. Girard, A. Bruyant, and A. Dereux, "SNOM signal near plasmonic nanostructures: an analogy with fluorescence decay channels," J. Microsc. (NFO9) **229**, 302–306 (2008).
27. A. Trügler and U. Hohenester, "Strong coupling between a metallic nanoparticle and a single molecule," Phys. Rev. B **77**, 115403 (2008).
28. W. Barnes, "Fluorescence near interfaces: the role of photonic mode density," J. Mod. Opt. **45**, 661–699 (1998).
29. C. S. Yun, A. Javier, T. Jennings, M. Fisher, S. Hira, S. Peterson, B. Hopkins, N. O. Reich, G. F. Strouse Nanometal Surface Energy Transfer in Optical Rulers, Breaking the FRET Barrier, J. Am. Chem. Soc. 127 (2005) 3115-3119.

1. Introduction

The precise control of the coupling efficiency between a quantum emitter (fluorescent molecule, quantum dot…) and a metallic nanoparticle is at the origin of the new field of *molecular plasmonics* [1]. In these composite systems, coupling with the molecule is mainly of electromagnetic origin, principally mediated by plasmon resonances. The optical properties of metallic nanoparticles are strongly relying on different plasmon–polaritons modes with specific properties. For instance, an elongated metallic particle can support both a dipolar (localised) plasmon mode characterized by high electromagnetic field confinement and an interface (propagating) plasmon mode able to guide electromagnetic energy along the particle surface. The strong confinement of the localised plasmon mode leads to a very efficient coupling with a nearby emitter. This coupling strength is at the origin of surface–enhanced spectroscopy. In addition, the excitation of the interface mode of the particle is responsible for transferring luminous energy away from the source of emission. By controlling the electromagnetic confinement at a nanorod extremity and understanding the propagation of the optical mode along its surface, it was recently proposed to realize an antenna in the optical domain [2, 3, 4]. Optical antennas are fundamental devices for interfacing light with nano-objects and could be used for instance to efficiently couple a single photon source to an optical fiber [4, 5]. Optimization of an optical antenna is a difficult problem since its spectroscopic response strongly depends on the shape, the chemical nature of the materials, and the surrounding environment. Among several methods available to describe the electromagnetic response of metallic particle of arbitrary shape, boundary element

#98208 - $15.00 USDReceived 1 Jul 2008; revised 22 Aug 2008; accepted 24 Aug 2008; published 17 Oct 2008

method [6], multiple multipole technique [7, 8], finite–difference time–domain simulations [9], and Green dyadic formalism [10] have been used to analyze the coupling between a fluorescent molecule and an optical antenna.

All these purely numerical studies however, can be supplemented by analytical approaches for which mathematical solutions exist. Indeed, an analytical study of simplified geometries can facilitate the description of the elementary processes involved in these coupled systems. Despite restricted shapes, *e.g.* spheres or ellipsoids, some important behaviors and trends can be identified [7, 8, 11, 12, 13, 14]. In a recent work, using a quasi-static model, Bharadwaj and Novotny discussed the optimal fluorescence wavelength and found that it should be red-shifted from the interface plasmon resonance of the particle [13]. In the same time, Mertens *et al* compared full electrodynamical theory to a corrected quasi-static model and demonstrated a trade–off between emitter-particle coupling, efficient for small spheres, and signal scattering, efficient for large particles [14]. They obtained an optimal sphere diameter around 50-100 nm, in the optical domain.

In this article, we address, from analytical arguments, the problem of optical near–field coupling processes governing the fluorescence of a molecule placed in the vicinity of a mesoscopic spherical metallic particle, i-e a nanoparticle with characteristic dimensions that are not very small compared to the emission wavelength. In particular, we precisely distinguish the radiative and non-radiative channels and clearly identify different coupling mechanisms. In section 2, we describe the asymptotic behavior of the decay rates in the very near-field of a metallic particle. The coupling of the emitter to the different plasmon modes is demonstrated from detailed analysis of the analytical expressions. The distance dependence of the decay rates is then investigated in section 3. Finally, we discuss in section 4 the fluorescence enhancement optimization.

2. Near-field behavior

Figure 1 describes the model we consider. A single emitter is placed at a distance z_0 from a spherical particle of radius a. The surrounding medium optical index is n_B. In the following, we adopt the classical point of view for the description of the decay rate. This model assumes that the fluorescent emission can be identified to the power emitted by a dipole $\mathbf{p_0}$ oscillating at the fluorescent frequency $\omega_0 = 2\pi c/\lambda_0$ in vacuum. Here the classical dipole represents twice the quantum transition dipole moment of the emitter. As demonstrated in [15], this model is appropriate for describing weak coupling regime. In this article, we also assume that the electromagnetic properties of the metallic particle are described by a bulk optical index n_S. For molecule–particle distance below one nanometer, non-local description of the optical index should be taken into account [16, 17].

2.1. Analytical formulation based on Mie's expansion

The decay rates of a molecule in presence of a spherical particle can be solved by using well–known Mie formalism [18, 19]. When they are normalized with respect to the decay rate γ_0 of the free molecule, total decay rates write [19]:

$$\frac{\gamma_\perp}{\gamma_0} = n_B \left\{ 1 + \frac{3}{2} Re \sum_{n=1}^{\infty} n(n+1)(2n+1) B_n \left[\frac{h_n^{(1)}(u)}{u} \right]^2 \right\}, \quad (1)$$

$$\frac{\gamma_\parallel}{\gamma_0} = n_B \left\{ 1 + \frac{3}{2} Re \sum_{n=1}^{\infty} (n+\frac{1}{2}) \left[B_n \left[\frac{\zeta_n'(u)}{u} \right]^2 + A_n [h_n^{(1)}(u)]^2 \right] \right\}, \quad (2)$$

#98208 - $15.00 USDReceived 1 Jul 2008; revised 22 Aug 2008; accepted 24 Aug 2008; published 17 Oct 2008

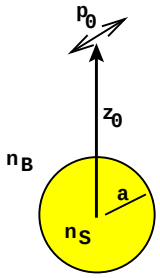

Fig. 1. Model used to study the molecule-particle coupling.

where the subscript $\perp$ ($\|$) indicates a dipole perpendicular (parrallel) to the particle surface and $u = k_B z_0 = 2\pi n_B z_0/\lambda_0$. For the sake of clarity, the analytical expressions of the Mie coefficients A_n and B_n will be detailed in the appendix. The two special functions $h_n^{(1)}$ and ζ_n that enter Eq. (1) and (2) represent the spherical Hankel and Ricatti–Bessel functions, respectively. Prime stands for differentiation with respect to u.

The radiative decay rates can be written as follows [19]:

$$\frac{\gamma_\perp^{rad}}{\gamma_0} = \frac{3n_B}{2}\sum_{n=1}^{\infty} n(n+1)(2n+1)\left|\frac{j_n(u)+B_n h_n^{(1)}(u)}{u}\right|^2, \tag{3}$$

$$\frac{\gamma_\parallel^{rad}}{\gamma_0} = \frac{3n_B}{4}\sum_{n=1}^{\infty}(2n+1)\left[|j_n(u)+A_n h_n^{(1)}(u)|^2+\left|\frac{\psi_n'(u)+B_n\zeta_n'(u)}{u}\right|^2\right], \tag{4}$$

where j_n is the spherical Bessel function and $\psi_n(u) = u\,j_n(u)$. From these four relations, the non–radiative decay rate can be obtained by computing the difference between total and radiative decay rates. Since we are interested in describing analytically the coupling process, we had to express this difference. Applying the procedure described in [20] in the presence of dielectric sphere to the present case of a metallic particle, we first develop the expressions (3) and (4) of radiative contributions to the relaxation rate. After some algebra, this leads to

$$\frac{\gamma_\perp^{rad}}{\gamma_0} = n_B+\frac{3n_B}{2}\sum_{n=1}^{\infty} n(n+1)(2n+1)\frac{|B_n h_n^{(1)}(u)|^2+2j_n(u)Re[B_n h_n^{(1)}(u)]}{u^2}, \tag{5}$$

$$\frac{\gamma_\parallel^{rad}}{\gamma_0} = n_B+\frac{3n_B}{4}\sum_{n=1}^{\infty}(2n+1)\left[\left|A_n h_n^{(1)}(u)\right|^2+2j_n(u)Re[A_n h_n^{(1)}(u)]+\frac{|B_n\zeta_n^{(1)}(u)|^2+2\psi_n'(u)Re[B_n\zeta_n^{(1)}(u)]}{u^2}\right]. \tag{6}$$

The non-radiative decay rates are now easily expressed as the difference between the total and

#98208 - $15.00 USDReceived 1 Jul 2008; revised 22 Aug 2008; accepted 24 Aug 2008; published 17 Oct 2008

radiative rates. After a few manipulations, we obtain

$$\frac{\gamma_\perp^{NR}}{\gamma_0} = \frac{\gamma_\perp}{\gamma_0} - \frac{\gamma_\perp^{rad}}{\gamma_0} = \frac{3n_B}{2}\sum_{n=1}^{\infty} n(n+1)(2n+1)\left|\frac{h_n^{(1)}(u)}{u}\right|^2\left[-Re(B_n)-|B_n|^2\right], \quad (7)$$

$$\frac{\gamma_\parallel^{NR}}{\gamma_0} = \frac{\gamma_\parallel}{\gamma_0} - \frac{\gamma_\parallel^{rad}}{\gamma_0} \quad (8)$$

$$= \frac{3n_B}{2}\sum_{n=1}^{\infty}(n+\frac{1}{2})\left[\left|\frac{\zeta_n^{(1)}(u)}{u}\right|^2\left[-Re(B_n)-|B_n|^2\right]+|h_n^{(1)}(u)|^2[-Re(A_n)-|A_n|^2]\right].$$

Let us note that the difference between the two terms proportional to $[-Re(B_n)]$ or $[-Re(A_n)]$ (extinction) and to $|B_n|^2$ or $|A_n|^2$ (scattering) directly relates to the energy conservation as discussed in section 2.2.1 [18]. Up to now, no assumption has been made on either the emitter-particle distance or the particle size. In the following section, we show how the expressions (1-8) simplify for short coupling distance regime.

2.2. Relaxation channels at very short distances

As recently discussed by Bharadwaj and Novotny [13], the non–radiative decay rate of a molecule is mainly dictated by an efficient coupling to the interface plasmon mode of the antenna whereas the radiative decay rate is associated to the excitation of a dipolar mode of the metallic particle. Indeed, in the very near–field, fluorescence relaxation processes are dominated by non-radiative transfer to the metal. It should be noted that for an emitter located at very short distance from the particle, the otherwise curved surface can be approximated by a flat interface. We therefore define the very near-field as the distance range such that $(z_0 - a) \ll a$. This criterion will be refined in section 3 devoted to the study of distance dependence of the decay rates.

The radiative channel, however, has other characteristics because it describes the power radiated in far–field zone by the whole *molecule plus particle* system. Since the particle dipolar mode presents the highest scattering cross–section, the radiative emission rate of the system may be similar to that of a molecule placed in the presence of a simple dipolar particle.

In the following, we will focus on the study of radiative and non–radiative contributions in the domain of the very short emitter-particle distances.

2.2.1. Nonradiative channel

At very short distances, the emitter-particle coupling relies mainly on the non-radiative channel. Using the asymptotic behavior of the spherical Bessel functions near zero [21], we can write from Eq. (7) and (8) respectively

$$\frac{\gamma_\perp^{NR}}{\gamma_0} \underset{u\to 0}{\sim} \frac{3n_B}{2u^3}\sum_{n=1}^{\infty}\frac{(n+1)^2}{u^{(2n+1)}}k_B^{2n+1}\left[Im(\alpha_n)-\frac{n+1}{n(2n-1)!!(2n+1)!!}k_B^{2n+1}|\alpha_n|^2\right], \text{and} \quad (9)$$

$$\frac{\gamma_\parallel^{NR}}{\gamma_0} \underset{u\to 0}{\sim} \frac{3n_B}{2u^3}\sum_{n=1}^{\infty}\frac{n(n+1)(n+1/2)}{(2n+1)u^{(2n+1)}}k_B^{2n+1}\left[Im(\alpha_n)-\frac{n+1}{n(2n-1)!!(2n+1)!!}k_B^{2n+1}|\alpha_n|^2\right], \quad (10)$$

#98208 - $15.00 USDReceived 1 Jul 2008; revised 22 Aug 2008; accepted 24 Aug 2008; published 17 Oct 2008

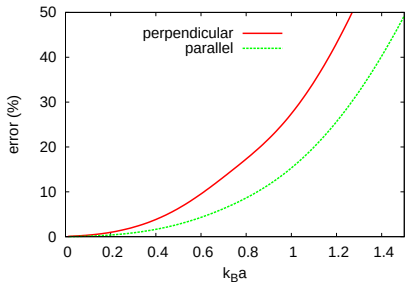

Fig. 2. Error done on the non radiative decay rate when approximated by Eq. (9) or (10) for a perpendicular or parallel orientation, respectively. The molecule is located 1 nm from a gold particle in air. The emission wavelength is $\lambda_0 = 580$ nm.

where $(2n+1)!! = 1\times 3\times 5...\times(2n+1)$ and we introduce the n^{th} order polarizability of the sphere

$$\alpha_n = \frac{n(\varepsilon_S-\varepsilon_B)}{(n+1)\varepsilon_B+n\varepsilon_S}a^{(2n+1)}. \tag{11}$$

Figure 2 represents the error done using the approximated expressions (9) or (10). The error is less than 10 % for $k_B a < 0.5$ and is around 20 % for mesoscopic particles ($k_B a \sim 1$).

Eq. (9) and (10) are an important result of this paper, since the non-radiative rate appears in a form that generalizes the expressions obtained previously with a purely dipolar sphere [22, 23], by including in a similar way all the particle modes. Moreover, within this formulation, the non radiative decay rate respects the optical theorem for each mode. More precisely, the first term in Eq. (9) or (10), proportional to $Im(\alpha_n)$, encodes the whole emission extinction, due to both absorption into the metallic particle and scattering in the far–field. The second term, proportional to $|\alpha_n|^2$ gives the fraction of power scattered by the particle itself. Hence, the non-radiated decay contribution is given by the difference between this two terms, as a direct consequence of the optical theorem [18, 22]. Finally, considering Eq. (9) and (10), it clearly appears that when the molecule approaches the metallic particle, it couples first to the dipole mode, then to multipole modes and finally to the interface plasmon mode for very short distances. This directly originates from the highest confinement of high order modes.

Terms $k_B^{2n+1}\alpha_n/u^{(2n+1)}$ are proportional to $(a/z_0)^{2n+1}$, therefore, when the emitter is placed in close vicinity to the particle ($z_0 \to a$), the high order terms [$\propto n^2(a/z_0)^{2n+1}$] dominate the expressions of the non-radiative decay rates. Under these conditions, Eq. (9) and Eq. (10) can be approximated by

$$\frac{\gamma_\perp^{NR}}{\gamma_0} \underset{z_0\to a}{\sim} \frac{3n_B}{2u^3}\frac{a}{z_0}Im\left(\frac{\varepsilon_S-\varepsilon_B}{\varepsilon_S+\varepsilon_B}\right)\sum_{n>>1} n^2\left(\frac{a}{z_0}\right)^{2n}, \tag{12}$$

$$\underset{z_0\to a}{\sim} \frac{3n_B}{8k_B^3}Im\left(\frac{\varepsilon_S-\varepsilon_B}{\varepsilon_S+\varepsilon_B}\right)\frac{1}{(z_0-a)^3} \tag{13}$$

$$\frac{\gamma_\parallel^{NR}}{\gamma_0} \underset{z_0\to a}{\sim} \frac{3n_B}{4u^3}\frac{a}{z_0}Im\left(\frac{\varepsilon_S-\varepsilon_B}{\varepsilon_S+\varepsilon_B}\right)\sum_{n>>1} n^2\left(\frac{a}{z_0}\right)^{2n}, \tag{14}$$

$$\underset{z_0\to a}{\sim} \frac{3n_B}{16k_B^3}Im\left(\frac{\varepsilon_S-\varepsilon_B}{\varepsilon_S+\varepsilon_B}\right)\frac{1}{(z_0-a)^3}. \tag{15}$$

Note that we used the fact that the serie diverges for $z_0 \simeq a$, so that the infinite serie sum reduces to its highest order term and can be compared to the serie expansion of $(1-a/z_0)^{-3}$ (see also

#98208 - $15.00 USDReceived 1 Jul 2008; revised 22 Aug 2008; accepted 24 Aug 2008; published 17 Oct 2008

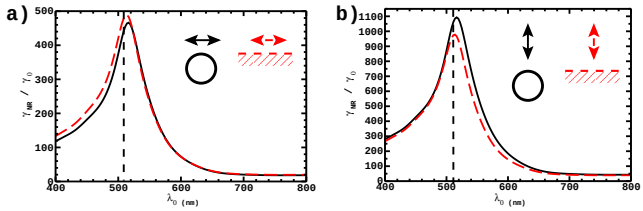

Fig. 3. Non radiative decay rate dependence for an emitter placed 5 nm above a gold nanoparticle (80 nm diameter) embedded in a PMMA matrix (solid line) or above a flat gold/PMMA interface film (dashed line, quasi-static approximation). (a) Dipole parallel to the surface. (b) Dipole perpendicular to the surface. Vertical lines indicate the Au/PMMA interface plasmon mode resonance.

[15]). Expressions (13) and (15) exactly reproduce the short range (quasi-static) behavior of non–radiative decay rate near a flat metal surface [24].

As a concrete example, we now consider a fluorescent molecule in presence of a 80 nm diameter gold nanoparticle ($a = 40$ nm) since similar systems were the topic of recent experimental [7, 11, 12] and theoretical works [8, 14]. The surrounding medium index is $n_B = 1.5$ corresponding to both PMMA (polymethylmethacrylate) and glass indices since molecule are generally dispersed into a PMMA matrix deposited on a glass substrate. Note that in this case, $k_B a \approx 0.3$ for emission wavelength in the visible range, corresponding to a particle of mesoscopic size. Figure 3 represents the wavelength dependence of the non radiative decay rate in the very near–field of a gold particle or a flat film. As expected, the non–radiative coupling to a spherical metallic particle is very well reproduced by assuming the quasi–static approximations (13) or (15). In both cases, a resonance occurs at $\lambda \simeq 515$ nm indicating a coupling to the interface plasmon mode.

2.2.2. Radiative channel

We apply a similar procedure to the radiative contribution. Taking the limit $u \to 0$ in expression (5), the radiative decay rate for a dipole perpendicular to the particle surface is given by

$$\frac{\gamma_\perp^{rad}}{\gamma_0} \underset{u\to 0}{\sim} n_B + \frac{3}{2u^2}\sum_{n=1}^{\infty} n(n+1)^2(2n+1)\left\{ \frac{n+1}{[(2n+1)!!]^2 u^{2n+2}} k_B^{4n+2}|\alpha_n|^2 + \frac{2}{[(2n+1)!!]^2 u} k_B^{2n+1} Re(\alpha_n) - \frac{2}{(2n-1)!![(2n+1)!!]^3} u^{2n} k_B^{2n+1} Im(\alpha_n) \right\}. \quad (16)$$

Numerical simulations (not shown) reveal an error up to 50 % for mesoscopic particles . The behavior of the radiative decay rate is drastically different from the non-radiative contributions in the very near-field of the particle. Having in mind that the polarizability depends on the sphere radius as a^{2n+1}, we note that the series converges to zero in the near-field range for small particle sizes. Therefore, the radiative decay rate can be reduced to the first terms only. Neglecting the last term in Eq. (16) compared to the two others, the radiative decay rate for a vertical dipole simplifies to

$$\frac{\gamma_\perp^{rad}}{\gamma_0} \underset{z_0\to a}{\sim} n_B \left\{ 1 + \frac{4}{z_0^3} Re(\alpha_1) + \frac{4}{z_0^6}|\alpha_1|^2 \right\} \quad (17)$$

#98208 - $15.00 USDReceived 1 Jul 2008; revised 22 Aug 2008; accepted 24 Aug 2008; published 17 Oct 2008

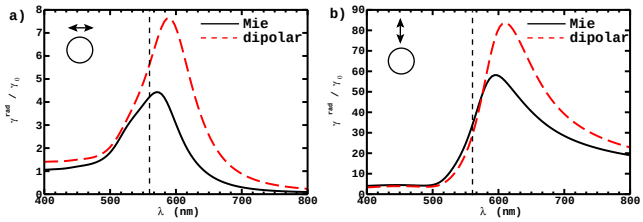

Fig. 4. Radiative decay rate for an emitter placed 5 nm above a gold nanoparticle (80 nm in diameter). (a) Dipole parallel to the surface. (b) Dipole perpendicular to the surface. The solid curves are calculated from Mie formalism (Eq. 3,4). The dashed curves assume a dipolar response of the particle, including finite size effects [Eq. 28) and (29) in appendix (6.2)]. Vertical lines indicate the sphere dipolar resonance.

which exactly reproduces the radiative contribution at small distance assuming a dipolar response of the metallic sphere (see *e.g* [23]). In case of a dipole parallel to the sphere surface, we obtain the following relation:

$$\frac{\gamma_{\parallel}^{rad}}{\gamma_0} \underset{z_0 \to a}{\sim} n_B \left\{ 1 - \frac{2}{z_0^3} Re(\alpha_1) + \frac{1}{z_0^6} |\alpha_1|^2 \right\}, \tag{18}$$

that is once again in agreement with a dipolar response of the metallic sphere. Note that these expressions slightly differ from the equation given in [23] by the absence of the radiation reaction term in the polarizability α_1. This term, which comes from the finite size of the particle, is necessary in order to satisfy the optical theorem. In a more critical way, a correct description of scattering resonances requires to include simultaneously both the radiation reaction term *and* a dynamic polarization term [25]. This can be easily achieved within the volume integral methods and leads to the following polarizability [26]

$$\alpha_{eff} = [1 - M_B \frac{\alpha_1}{a^3}]^{-1} \alpha_1 \tag{19}$$

$$M_B = 2[(1 - ik_B a)e^{ik_B a} - 1] \tag{20}$$

where α_1 is the static polarizability as defined in Eq. (11) and the dipolar response $\mathbf{p}$ of the particle to an external electric field $\mathbf{E}_0$ obeys $\mathbf{p} = 4\pi\varepsilon_0\varepsilon_B\alpha_{eff}\mathbf{E}_0$.

As shown on Fig. 4, the dipolar model qualitatively reproduces the wavelength dependence of the radiative decay rates. Clearly, the resonances are red-shifted compared to the dipolar mode frequency ω_1 ($\lambda_1 = 2\pi c/\omega_1 = 560$ nm). More precisely, the resonance is only slightly red-shifted in case of a dipole parallel to the particle surface ($\lambda = 570$ nm instead of $\lambda_1 = 560$ nm), whereas a stronger deviation is observed for a dipole perpendicular to the surface of the metallic particle ($\lambda = 595$ nm). This red–shift is due to a more important dipole–dipole coupling between the molecule and the gold particle for this dipole orientation. The efficiency of dipole-dipole coupling also explains the higher decay rate obtained when considering dipolar response of the particle compared to Mie description in which the energy is dispersed on all modes. Let us also note that the distance dependence of the radiative decay rate should strongly depends on the emission wavelength. Far from any resonance, the amplitude of the particle dipole is proportional to the field emitted by the emitter. Consequently, a z_0^{-3} dependence is expected for a particle in the near-field of the quantum emitter. As already discussed in [23], an additional Förster–type dependence contribution (z_0^{-6}) is expected close to the particle resonance because a strong dipole–dipole coupling dominates between the particle and the emitter. Note that in this case, a corrective term should be added to properly describe the whole decay rate [15, 27].

#98208 - $15.00 USDReceived 1 Jul 2008; revised 22 Aug 2008; accepted 24 Aug 2008; published 17 Oct 2008

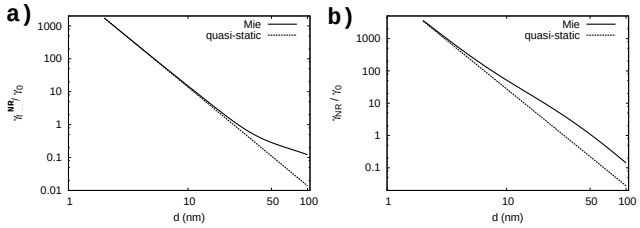

Fig. 5. Non radiative decay rates as a function of the distance $d = (z_0 - a)$ to the particle surface (solid lines) or gold flat film (dashed lines, quasi-static approximation) for a parallel (a) and perpendicular (b) dipole. The emission wavelength is $\lambda_0 = 580$ nm.

3. Distance dependence

In this section, we have chosen the emission wavelength $\lambda_0 = 580$ nm of the terrylene molecule. This molecule is widely used in single molecule spectroscopy experiments and the position of emission wavelength ensures that both the parallel and perpendicular radiative channels should be strongly enhanced. The embedding medium is again PMMA. We compare the distance dependence to the two limiting cases (quasi-static flat surface and dipolar particle) introduced in the previous section. Exact expressions of the different decay rates are given in the appendix.

Figure 5 represents the non radiative decay rate variation when increasing the particle–molecule distance. The quasi-static approximation remains satisfying only below 10 nm, corresponding to $d/a < 0.2$ as the range where the spherical surface can be approximated by a flat interface. As expected, a d^{-3} law is observed for these very short distance corresponding to the creation of an exciton in the bulk of the metal [28]. Note that a d^{-4} law can be expected for even shorter distances, due to the creation of an exciton at the metal surface [29]. Such a description needs to properly describe the metal/dielectric interface and to take into account the nonlocals effect into the metal dielectric constant [28].

We now consider the radiative contribution to the decay rate, and compare it to a dipolar response of the particle (Fig. 6). In order to improve the comparison accuracy, we include finite size effects into the polarizability. The dipolar model only qualitatively reproduces the radiative decay rate behavior, indicating that higher plasmonic modes are involved in the radiative process [14]. At large distances, however, the dipolar mode is sufficient to describe the radiative emission evolution, as far as finite size effects are properly included. Finally, we do not observe simple distance dependence law for small separation distance since the two z_0^{-3} and z_0^{-6} processes compete [23].

4. Fluorescence enhancement and particle size effect

In this last section, we discuss the influence of the particle size on the fluorescent enhancement for a molecule coupled to a gold particle. The fluorescence intensity enhancement is given by

$$\eta_{fluo}(\mathbf{r_0}) = |\mathbf{u}\cdot\mathbf{E}(\lambda_{exc},\mathbf{r_0})|^2 \frac{\gamma^{rad}(\mathbf{r_0})}{\gamma(\mathbf{r_0})}, \tag{21}$$

where $\mathbf{E}$ is the normalized electric field computed at the molecule location $\mathbf{r_0}$ from Mie theory [18] at the excitation wavelength λ_{exc} and γ^{rad}/γ represents the quantum efficiency. $\mathbf{u}$ indicates the orientation of the molecule transition dipole moment.

A critical parameter for fluorescence enhancement is position of both the excitation and emission wavelengths compared to the plasmon modes resonances [8, 13]. Indeed, the excited field mainly couples to the dipolar mode and therefore strongly depends on the particle size, as

#98208 - $15.00 USDReceived 1 Jul 2008; revised 22 Aug 2008; accepted 24 Aug 2008; published 17 Oct 2008

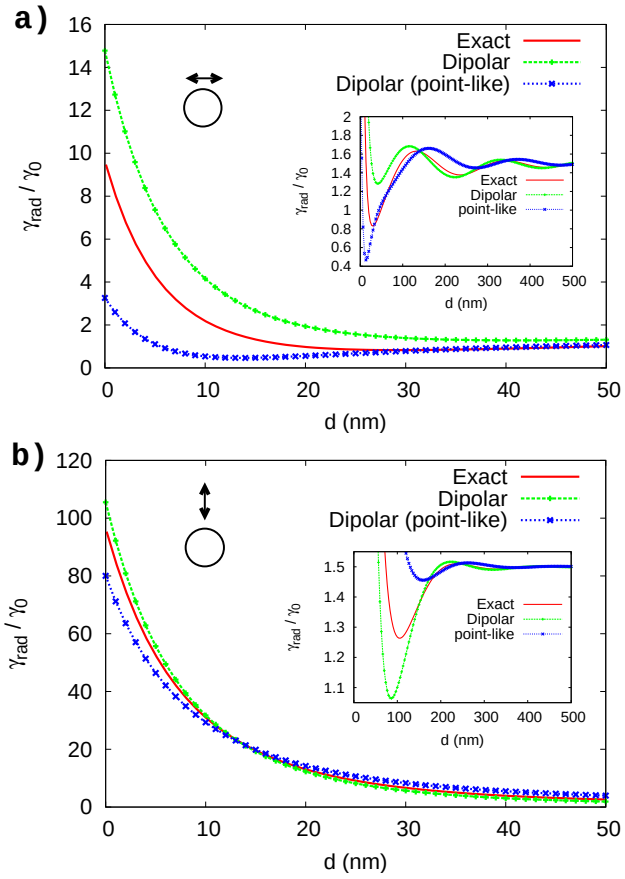

Fig. 6. Radiative decay rate dependence with respect to the distance d between the particle and the molecule: for a dipole (a) parallel or (b) perpendicular to the particle surface. *'Exact'* curves refers to Mie formalism (Eq. 3,4), *'dipolar'* corresponds to a dipolar model, including finite size effects [Eq. 28) and (29) in appendix (6.2)] and *'dipolar (point–like)'* assumes a point–like dipolar response of the particle to an external field [(Eq. 28) and (29) where α_{eff} is approximated by α_1]. The insets show far-field behaviours. The emission wavelength is $\lambda_0 = 580$ nm.

#98208 - $15.00 USDReceived 1 Jul 2008; revised 22 Aug 2008; accepted 24 Aug 2008; published 17 Oct 2008

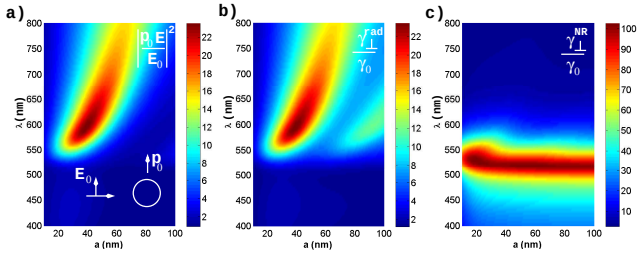

Fig. 7. Normalized electric-field intensity (a), decay rate (b) and non-radiative rate (c) calculated 10 nm away the particle surface as a function of both wavelength and particle radius. The system is shown in the inset of Fig. 7(a). The molecule is oriented perpendicularly to the sphere surface.

shown by Eq. (19). Moreover, as discussed above, the radiative decay rate also mainly originates from coupling to the dipolar mode. However, due to dipole-dipole coupling, an additionnal redshift occurs, particularly for dipole perpendicular to the particle surface (see Fig. 4). On the contrary, the non-radiative rate is governed by interface mode so that it does almost not depend on the particle size for small emitter-particle coupling distances.

We consider again a gold nanoparticle embedded in PMMA coupled to a fluorescent molecule. The molecule is perpendicular to the particle surface since strongest effects are expected in this case. Figure 7(a) represents the excitation field intensity near the particle in function of both the particle size and the excitation wavelength. Figures 7(b) and 7(c) show respectively the radiative (Eq. 5) and non-radiative (Eq. 7) decay rates when varying emission wavelength and also the particle radius. Independent of the particle size, the non radiative channel is resonantly opened for emission wavelengths around $\lambda_0 = 515$ nm (see Fig. 7(c)) due to coupling to the interface mode. As expected, the excitation intensity (Fig. 7(a)) and the radiative decay rate (Fig. 7(b)) present very similar behaviors, closely related to the dipolar mode of the metallic particle. Let us note, however, that for particle radius above $a \approx 80$ nm, the radiative channel also couples to quadrupolar mode as can be seen on Fig. 7(b) [14].

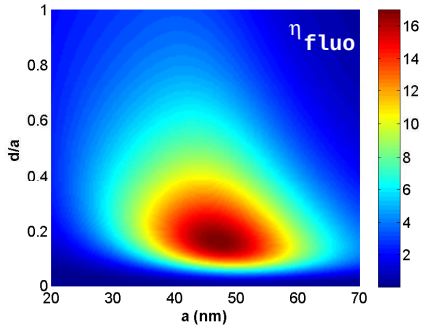

Fig. 8. Fluorescent enhancement for 'DiD-gold particle' coupled system embedded in PMMA.

Therefore, strong fluorescent enhancement can be expected for a molecule–particle coupled system such that: i) the absorption wavelength is close to the particle dipolar resonance to enhance the excitation field, ii) the emission wavelength is far from the interface mode resonance to reduce ohmic losses and iii) the particle is small enough to avoid molecule coupling to the quadrupolar mode resonance and strongly enhance the radiative channel. Finally, we consider

#98208 - $15.00 USDReceived 1 Jul 2008; revised 22 Aug 2008; accepted 24 Aug 2008; published 17 Oct 2008

a specific dye molecule, namely DiD which presents absorption and emission peaks around $\lambda_{exc} = 635$ nm and $\lambda = 665$ nm respectively. Figure 8 presents the fluorescent enhancement for several particle radius, in function of the emitter-particle distance. A strong 17 fold enhancement is observed for radius $40nm < a < 50nm$ at separation distance around $d \approx 8$ nm ($d/a \approx 0.2$). It is worthwile to note here that matching the excitation and detection wavelengths to the molecule absorption and emission peaks respectively, we profit from both the molecule absorption and fluorescence cross-sections and also fluorescence enhancement due to coupling to the metallic particle.

5. Conclusion

In summary, we have theoretically and numerically investigated the decay rate of an emitter coupled to a mesoscopic metallic particle. By starting from an asymptotic expansion of the different decay rate contributions in the very near–field of a spherical metallic particle, we demonstrated that the non–radiative channel process is associated with a coupling to the interface plasmon mode of the particle whereas the radiative decay rate process involves a transfer to dipolar plasmon mode. We have examined the extent of these couplings and compared it with two asymptotic models: a flat metal surface and a dipolar response of the particle. We found a red-shift of the radiative decay rate due to dipole-dipole coupling between the molecule and the particle. We also demonstrated that near-field coupling can be expressed in a simple form that obeys optical theorem for each particle mode. These results show that a deep understanding of the complex fluorescence decay mechanisms can be obtained from a simple and analytical model. Finally, it provides some guidelines for optimizing the particle size to enhance the molecular fluorescence.

Acknowledgements

This work is partially supported by the Agence Nationale de la Recherche (ANR) (project ANTARES, PNANO07-51) and the European Network of Excellence PlasmoNanoDevices (contract No 507879).

6. Appendix

To facilitate the reading of this article, we reproduce in this appendix the various expressions of the decay rates assuming a dipolar response of the spherical particle. These expressions can be easily deduced from the classical description of the spontaneous emission rates and can be found in the literature.

6.1. Mie coefficients

An exact description of the particle electromagnetic response to an external field needs to properly describe all the particle modes. The n^{th} mode contribution depends on the two Mie scattering coefficients A_n and B_n [18, 19] ($k_B = 2\pi n_B/\lambda_0$ and $k_S = 2\pi n_S/\lambda_0$ are the wavenumbers into the embedding medium and the sphere, respectively)

$$A_n = \frac{j_n(k_B a)\psi_n'(k_S a) - j_n(k_S a)\psi_n'(k_B a)}{j_n(k_S a)\zeta_n'(k_B a) - h_n^{(1)}(k_B a)\psi_n'(k_S a)}, \tag{22}$$

$$B_n = \frac{\varepsilon_B j_n(k_B a)\psi_n'(k_S a) - \varepsilon_S j_n(k_S a)\psi_n'(k_B a)}{\varepsilon_S j_n(k_S a)\zeta_n'(k_B a) - \varepsilon_B h_n^{(1)}(k_B a)\psi_n'(k_S a)}. \tag{23}$$

where j_n and $h_n^{(1)}$ are the usual spherical Bessel and Hankel functions, and $\psi_n(z) = z j_n(z)$ and $\zeta_n(z) = z h_n^{(1)}(z)$ the Ricatti-Bessel functions [18, 21].

#98208 - $15.00 USDReceived 1 Jul 2008; revised 22 Aug 2008; accepted 24 Aug 2008; published 17 Oct 2008

6.2. Dipolar spherical particle

The total decay rates write [22, 23, 26]

$$\frac{\gamma_{\parallel}}{\gamma_0} = n_B \left\{ 1 + \frac{3k_B^3}{2} Im \left[\alpha_{eff} e^{2iu} (\frac{1}{u} + \frac{i}{u^2} - \frac{1}{u^3})^2 \right] \right\}, \tag{24}$$

$$\frac{\gamma_{\perp}}{\gamma_0} = n_B \left\{ 1 + 6k_B^3 Im \left[\alpha_{eff} e^{2iu} (\frac{1}{u^3} - \frac{i}{u^3})^2 \right] \right\}, \tag{25}$$

where α_{eff} is the particle effective polarizability associated to the dipolar mode, including finite size effects as expressed by Eq. (19). The non radiative decay rates write

$$\frac{\gamma_{\parallel}^{NR}}{\gamma_0} = \frac{3n_B}{2} k_B^3 \left[Im(\alpha_{eff}) - \frac{2k_B^3}{3} |\alpha_{eff}|^2 \right] \left[\frac{1}{u^2} - \frac{1}{u^4} + \frac{1}{u^6} \right], \tag{26}$$

$$\frac{\gamma_{\perp}^{NR}}{\gamma_0} = 6k_B^3 n_B \left[Im(\alpha_{eff}) - \frac{2k_B^3}{3} |\alpha_{eff}|^2 \right] \left[\frac{1}{u^4} + \frac{1}{u^6} \right]. \tag{27}$$

Then the radiative decay rates are calculated as the difference between the total and the non radiative decay rates:

$$\frac{\gamma_{\perp}^{rad}}{\gamma_0} = \frac{\gamma_{\perp}}{\gamma_0} - \frac{\gamma_{\perp}^{NR}}{\gamma_0} \tag{28}$$

$$\frac{\gamma_{\parallel}^{rad}}{\gamma_0} = \frac{\gamma_{\parallel}}{\gamma_0} - \frac{\gamma_{\parallel}^{NR}}{\gamma_0}. \tag{29}$$

#98208 - $15.00 USD Received 1 Jul 2008; revised 22 Aug 2008; accepted 24 Aug 2008; published 17 Oct 2008